

# Icosahedral phase formation in rapidly quenched aluminum–ruthenium alloys

Steven M. Anlage<sup>a)</sup> and Brent Fultz

*Applied Physics and Materials Science, California Institute of Technology, Pasadena, California 91125*

Kannan M. Krishnan

*National Center for Electron Microscopy, Lawrence Berkeley Laboratory, Berkeley, California 94720*

(Received 6 April 1987; accepted 8 February 1988)

Systematic rapid quenching experiments on the icosahedral phase-forming system  $\text{Al}_{1-x}\text{Ru}_x$  were performed for  $x < 20$  at. %. The solidified alloys have been studied by electron microscopy and x-ray diffraction to determine their composition, constituent phases, and phase morphology. It has been determined that the icosahedral phase must form directly from the liquid and, at these quench rates, is always found in the presence of second or third phases. The results have been summarized in a metastable phase diagram appropriate for rapid solidification of  $\text{Al}_{1-x}\text{Ru}_x$  at piston and anvil quench rates. This metastable phase diagram describes the results for Ru concentrations less than 14 at. %.

## I. INTRODUCTION

A novel material, containing precipitates displaying icosahedral point group symmetry in electron diffraction, along with quasiperiodic translational order, has recently been formed by rapid solidification.<sup>1</sup> There is a great deal of interest in studying this icosahedral phase to determine its atomic structure and physical properties.<sup>2</sup> Naturally one is also interested in understanding and controlling the mechanisms responsible for the formation and growth of the icosahedral phase. With this in mind, we have performed rapid solidification experiments on one icosahedral phase-forming alloy system, with the intention of determining its end-product phases as a function of composition.

We have chosen the aluminum–ruthenium alloy system because of the relative simplicity of its equilibrium phase diagram in the icosahedral phase-forming region. The  $\text{Al}_{1-x}\text{Ru}_x$  system has only three equilibrium phases for  $x < 25$  at. % Ru, namely,  $\text{Al}_{13}\text{Ru}_4$ ,  $\text{Al}_6\text{Ru}$ , and the fcc Al–Ru solid solution.<sup>3</sup> In Ref. 3 it was also found that nucleation and growth of the  $\text{Al}_6\text{Ru}$  phase was kinetically bypassed even at cooling rates of less than 20 K/s. Because of this, icosahedral phase formation proves to be relatively easy in the broad regime  $2.4 < x < 23.5$  at. % Ru.

## II. EXPERIMENTAL PROCEDURE

Alloys of aluminum and ruthenium were formed by inductively heating the elemental metals in an alumina crucible contained within a high-purity argon atmo-

sphere. The homogeneous ingots were subsequently quenched by the piston and anvil technique.<sup>4</sup> This quenching technique involves rapid thermal transfer from two sides of the sample, and produces more uniform cooling conditions than melt spinning. Quench rates are estimated to be  $10^5$ – $10^6$  K/s.<sup>5</sup> Alloys of all compositions were quenched under nearly identical conditions of piston impact velocity and peak temperature above the melting point.

Alloys  $\text{Al}_{1-x}\text{Ru}_x$  for  $x = 2.5, 5, 7.5, 10,$  and  $12.5$  at. % were subsequently studied by transmission electron microscopy (TEM). These samples were cut into 3 mm disks and thinned to electron transparency by electrochemical jet polishing with a solution of methanol and perchloric acid at  $-40^\circ\text{C}$ . The samples were then ion milled at a shallow angle to remove organic deposits and oxides left over from the chemical thinning process. The TEM work was performed on a Phillips EM430 scanning transmission electron microscope (STEM) operated at 300 kV and equipped with an EDAX energy dispersive x-ray analysis unit, as well as on a JEOL 200CX STEM operated at 200 kV with a Kevex x-ray analysis unit. Through the manufacturers' software, the intensities of the Al K peaks and Ru L peaks were determined and converted into chemical concentrations. Energy dispersive x-ray analysis was performed at selected spots as well as on a line of spots through an icosahedral particle and into its neighboring matrix. Some alloy compositions were checked by atomic absorption spectrometry, and these data were used for obtaining small corrections to the chemical composition data from energy dispersive x-ray analysis. Alloys  $\text{Al}_{1-x}\text{Ru}_x$  for  $x = 14, 15, 17.5,$  and  $20$  at. % were not examined by TEM because of their brittleness, but were studied only by Cu  $K_\alpha$  x-ray diffractometry.

<sup>a)</sup> Present Address: Department of Applied Physics, Stanford University, Stanford, California 94305.

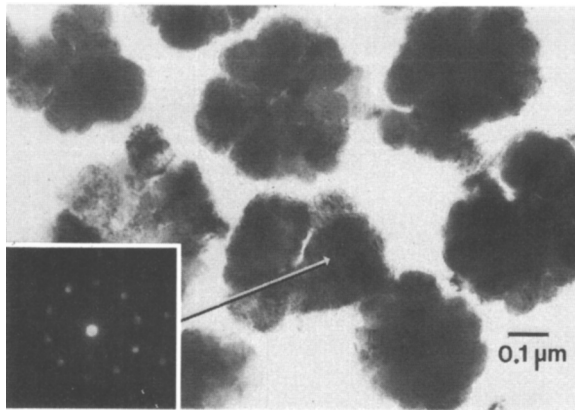


FIG. 1. Bright-field transmission electron microscope image of a piston and anvil liquid-quenched  $Al_{90}Ru_{10}$  alloy showing the rosette shaped icosahedral particles surrounded by aluminum matrix. An arrow shows the approximate location where the fivefold diffraction pattern (inset) was obtained.

### III. OBSERVATIONS

The icosahedral phase was found by TEM or x-ray analysis in all of the rapidly solidified alloys studied. Figures 1 and 2 show the general morphologies of two of these rapidly solidified alloys. Analytical STEM analysis of the icosahedral phase particles showed that they contain concentrations of ruthenium well above the nominal composition of the alloy, and the surrounding matrix is depleted in ruthenium. The particles in rapidly quenched  $Al_{90}Ru_{10}$  (Fig. 1),  $Al_{92.5}Ru_{7.5}$ , and  $Al_{95}Ru_5$  show the characteristic rosette structure seen in most other Al-transition metal icosahedral phase-forming

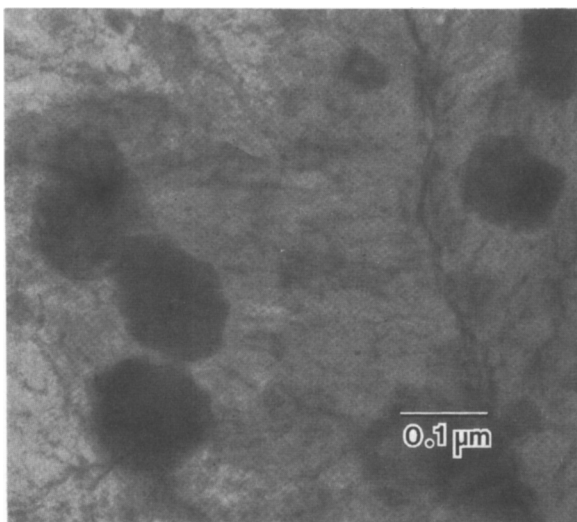


FIG. 2. Bright-field transmission electron microscope image of a piston and anvil liquid-quenched  $Al_{97.5}Ru_{2.5}$  alloy showing the equiaxed icosahedral particles surrounded by an aluminum matrix.

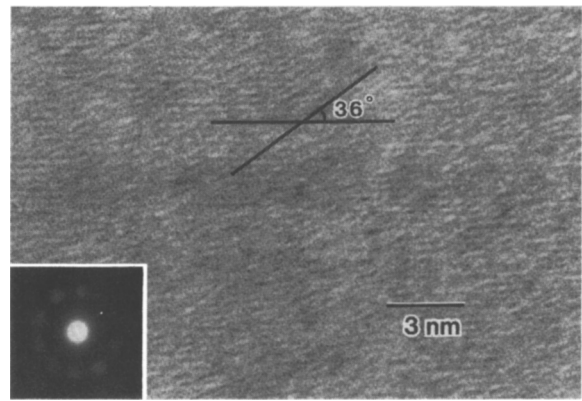


FIG. 3. Transmission electron microscope lattice fringe image of an icosahedral particle in piston and anvil-quenched  $Al_{97.5}Ru_{2.5}$ . The image was constructed from the bright ring of spots (inset) obtained by convergent beam diffraction.

systems. On the other hand, particles of icosahedral phase in  $Al_{97.5}Ru_{2.5}$  (Fig. 2) do not form rosettes, but have a simple equiaxed shape. A lattice fringe image of one such grain of  $Al_{97.5}Ru_{2.5}$  is shown in Fig. 3. The image clearly shows fringes crossing at angles of  $36^\circ$ , characteristic of the icosahedral phase.

The composition of the icosahedral phase was determined to be approximately 19 at. % Ru from energy dispersive x-ray analysis of the grains in rapidly solidified  $Al_{1-x}Ru_x$  for  $0.025 \leq x \leq 0.10$ . The fact that the icosahedral grains in  $Al_{97.5}Ru_{2.5}$  (Fig. 2) have a composition of 19 at. % Ru is evidence for very strong segregation of Ru into the icosahedral particles during the rapid quench.

X-ray diffractometry (XRD) of rapidly solidified  $Al_{86}Ru_{14}$  showed the presence of both the Al-Ru icosahedral phase and the Al-Ru fcc solid solution. An XRD pattern of rapidly quenched  $Al_{85}Ru_{15}$  showed that Al,

TABLE I. Results of a systematic rapid quenching experiment on the Al-Ru alloy system. Here Al is the Al-Ru solid solution, IP is the Al-Ru icosahedral phase, TEM and XRD represent transmission electron microscopy and x-ray diffraction analysis, respectively.

Sample composition	Phases present	Analysis technique
$Al_{97.5}Ru_{2.5}$	Al + IP	TEM, XRD
$Al_{95}Ru_5$	IP + Al	TEM, XRD
$Al_{92.5}Ru_{7.5}$	IP + Al	TEM, XRD
$Al_{90}Ru_{10}$	IP + Al	TEM, XRD
$Al_{87.5}Ru_{12.5}$	IP + Al	TEM, XRD
$Al_{86}Ru_{14}$	IP + Al	XRD
$Al_{85}Ru_{15}$	$Al_{13}Ru_4$ + IP + Al	XRD
$Al_{82.5}Ru_{17.5}$	$Al_{13}Ru_3$ + IP + Al	XRD
$Al_{80}Ru_{20}$	$Al_{13}Ru_4$ + IP + Al	XRD

Al–Ru icosahedral phase, and  $\text{Al}_{13}\text{Ru}_4$  were all present in substantial amounts. This three-phase material was observed in a binary alloy under conditions of constant temperature and pressure, in violation of the Gibbs phase rule. Hence it is impossible to represent the results of this quench on a single equilibrium or metastable equilibrium<sup>6</sup> phase diagram. Finally, XRD analysis of rapidly quenched  $\text{Al}_{80}\text{Ru}_{20}$  revealed that the alloy is mostly  $\text{Al}_{13}\text{Ru}_4$  with a smaller amount of icosahedral material. In all of the alloys studied, we have never found an example of single-phase icosahedral material made by rapid quenching from the liquid.

The results of all the rapid quenching experiments are summarized in Table I. The product phases are listed in the order that they are expected to form during the quench (see Sec. IV).

#### IV. DISCUSSION

In Fig. 4 we present a schematic metastable equilibrium phase diagram (appropriate for liquid quenching by the piston and anvil technique<sup>4,5</sup>) as well as the equilibrium phase diagram<sup>3</sup> for the Al–Ru system. Because the rapidly quenched Al–Ru samples contained up to three phases, we cannot represent the results of our experiments on a single stable or metastable equilibrium binary phase diagram. The phase diagrams shown in Fig. 4 can be used to predict the solid phases resulting from a rapidly solidified Al–Ru liquid.

The range of validity of each diagram, as well as the formation range of each product, are shown by the bars between the diagrams. The metastable phase diagram on the top of Fig. 4 is valid for Ru concentrations shown by the top bar. The solid portion of the bar represents concentrations where the diagram is exclusively correct, and the heavily dashed bar represents concentrations where it must be used in conjunction with the equilibrium diagram. A similar interpretation holds for the equilibrium phase diagram on the bottom of Fig. 4, where the lightly dashed bar indicates Ru concentrations for which the equilibrium phase diagram does not apply to our work. One can think of the equilibrium phase diagram as being valid for very slow quench rates, while the metastable equilibrium phase diagram, used in conjunction with the equilibrium phase diagram, allows one to interpret phases obtained with piston and anvil quench rates.

The phase diagrams in Fig. 4 show four solid phases: an Al–Ru solid solution that extends to 2.4 at. % Ru,<sup>7</sup> the  $\text{Al}_6\text{Ru}$  compound,<sup>8</sup> the icosahedral phase, and the well-characterized compound  $\text{Al}_{13}\text{Ru}_4$ .<sup>9</sup> We have represented the icosahedral phase ( $\approx 19$  at. % Ru) on the metastable phase diagram as a compound, since there is evidence that it forms by nucleation and growth rather than through kinetic freezing of the liquid.<sup>10</sup> The icosahedral compound is shown with a wide

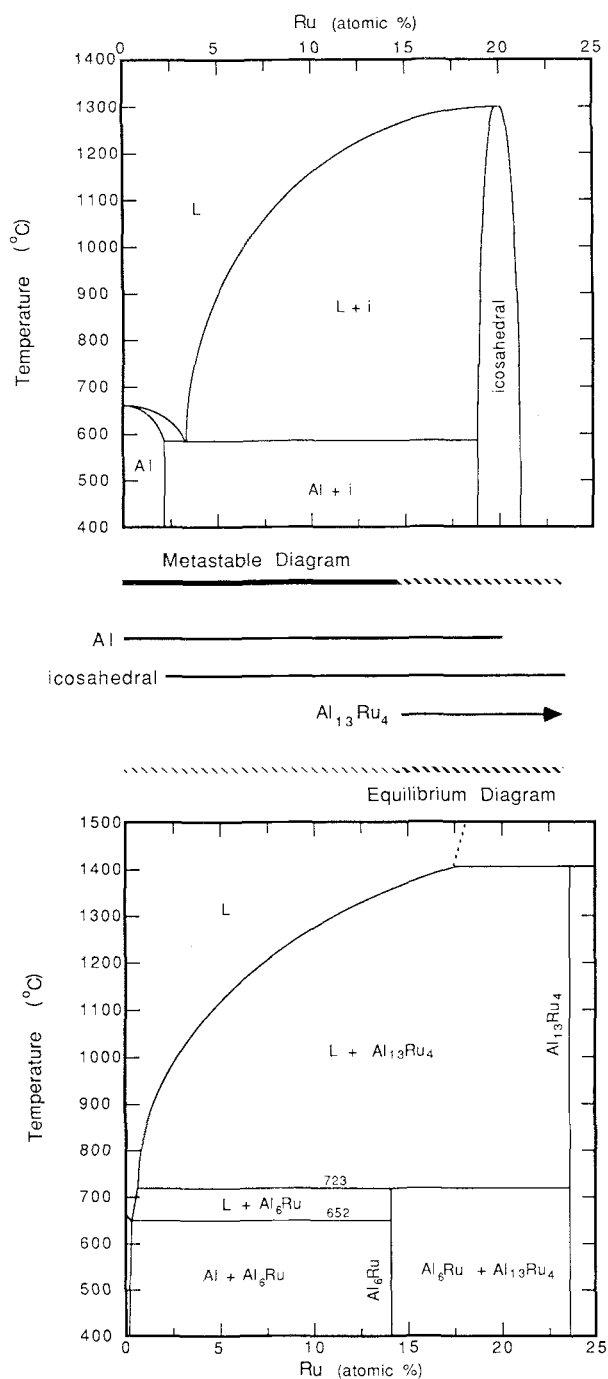


FIG. 4. Schematic metastable phase diagram appropriate for the kinetic constraints imposed by liquid quenching by the piston and anvil technique (top) and the equilibrium phase diagram (bottom) for the  $\text{Al}_{1-x}\text{Ru}_x$  system ( $x < 25$  at. % Ru). The uppermost and lowermost bars indicate the compositions over which the metastable and equilibrium phase diagrams represent the results of the rapid quenching experiments, respectively. The phases formed upon rapid quenching are indicated by the three bars at center.

phase field since it is known to be somewhat tolerant of chemical disorder.<sup>11</sup> Energy dispersive x-ray analysis line scans through the icosahedral particles showed some enhancement of Ru concentration near the centers

of the particles. For this reason, the icosahedral phase region in Fig. 4 has been made to widen slowly at lower temperatures. However, the difference in composition between the edge and center of the particles was 2.5 at. % Ru, which is only slightly greater than the resolution of these measurements.

On the bottom of Fig. 4 is the recently determined equilibrium phase diagram for the Al–Ru system.<sup>3</sup> It is found that peritectic growth of  $\text{Al}_6\text{Ru}$  is easily bypassed on cooling from the melt at quench rates of less than 20 K/s.<sup>3</sup> In the metastable phase diagram, we have drawn the metastable liquidus and eutectic significantly below those of their equilibrium counterparts to suggest that a significant amount of undercooling is taking place during the piston and anvil quench. Since the degree of undercooling has not been measured during the piston and anvil quench, the temperature values shown are schematic. Nevertheless, it is known that when metastable compounds form during a rapid quench that suppresses the formation of an equilibrium compound, the temperature of formation of the metastable phase must lie below that of the equilibrium compound.<sup>6</sup> For  $x \leq 14$  at. % Ru, formation of both the  $\text{Al}_{13}\text{Ru}_4$  and  $\text{Al}_6\text{Ru}$  phases is suppressed. Hence we can use as an upper limit on the metastable liquidus curve of the Al–Ru icosahedral phase the equilibrium liquidus of  $\text{Al}_{13}\text{Ru}_4$ .

We can establish a lower bound on the metastable icosahedral liquidus through an estimate made by another nonequilibrium measurement. Knapp and Follstaedt have performed rapid thermal annealing and quenching experiments by means of electron-beam treatments of thin films of icosahedral Al–Mn.<sup>12</sup> With this technique, they have measured the temperature  $T_0$  at which the Gibbs free energies of the icosahedral phase and the Al–Mn liquid at the same composition are equal. Knapp and Follstaedt have applied this technique to the Al–Ru icosahedral phase as well, and determined that  $T_0 = 1230 \pm 40$  °C.<sup>13</sup> Formation of the icosahedral phase below the temperature  $T_0$  will result in partitionless solidification,<sup>6</sup> producing single-phase icosahedral materials (which is not observed). Hence  $T_0$  is a lower limit for the formation temperature of the icosahedral phase. The metastable equilibrium liquidus for the Al–Ru icosahedral phase in Fig. 4 is drawn subject to these constraints.

According to the metastable phase diagram in Fig. 4, during a quench in the region  $3 < x < 14$  at. % Ru, the icosahedral phase forms directly from the liquid, until the eutectic temperature is reached (somewhat below 660 °C). At this point the liquid freezes to form a matrix surrounding the isolated icosahedral grains, resulting in a two-phase mixture of Al–Ru icosahedral phase and Al–Ru solid solution. For  $x < 3$  at. % Ru some of the Al–Ru solid solution will solidify first and then the Al–Ru icosahedral phase will be produced eutectically.

This may account for the observed difference in morphology of the icosahedral grains between the 10 at. % and 2.5 at. % Ru samples shown in Figs. 1 and 2. (This observation is the basis for placing the eutectic composition at 3 at. % Ru.)

We have found for alloy compositions in the range  $x > 14$  at. % Ru that the  $\text{Al}_{13}\text{Ru}_4$  phase is abundant in the rapidly quenched alloys. The substantial presence of  $\text{Al}_{13}\text{Ru}_4$  in an alloy of 15 at. % Ru suggests that the equilibrium phase diagram shown on the bottom of Fig. 4 must be included for a complete interpretation of the results. The metastable phase diagram describes our results for ruthenium concentrations less than 14 at. %, but the formation of the equilibrium compound  $\text{Al}_{13}\text{Ru}_4$  must be considered for higher ruthenium concentrations. We suspect that the formation of the  $\text{Al}_{13}\text{Ru}_4$  compound competes with the formation of the icosahedral phase, and the formation of  $\text{Al}_{13}\text{Ru}_4$  becomes significant at piston and anvil quench rates for alloy compositions with  $x > 14$  at. % Ru. Finally, for  $20 < x < 23.5$  at. % Ru a two-phase icosahedral and  $\text{Al}_{13}\text{Ru}_4$  mixture is expected to form upon rapid quenching, but this composition range was not explored in the present work.

Chemical composition measurements made by energy dispersive x-ray analysis show that the rapidly quenched samples exhibit a pronounced segregation of Ru into the icosahedral grains. The strong segregation of Ru to particles of the icosahedral phase implies a large diffusivity for Ru. If we define a diffusion length  $r_d$  such that all Ru in excess of the matrix solubility diffuses over this length to a particle of the icosahedral phase, we have the relationship,

$$r_d = r_p [(x_i - x_0)/(x - x_0)]^{1/3},$$

where  $r_p$  is the radius of the (spherical) icosahedral particle,  $x_i$  is its concentration of Ru,  $x$  is the Ru concentration in the bulk alloy, and  $x_0$  is the concentration of Ru in the Al matrix. Through x-ray chemical analysis, we have found the concentration  $x_i = 0.19$  for all alloys with Ru concentrations  $x$  between 0.025 and 0.10. We measured  $r_p$  for the largest particles found in TEM micrographs of each alloy.<sup>14</sup> We find that the volume of the largest icosahedral phase particles present increases linearly with alloy concentration  $x$ . A value of  $x_0 = 0.024$  was determined as the concentration at which the volume of icosahedral phase particles extrapolates to zero (i.e., the concentration at which only the Al–Ru solid solution is present). From the formula above, we calculate  $r_d \approx 0.5$   $\mu\text{m}$  for all alloy compositions between 0.025 and 0.10. Assuming a diffusion time of  $10^{-4}$  s during rapid cooling,<sup>5</sup> we deduce a diffusivity for Ru of approximately  $10^{-5}$   $\text{cm}^2/\text{s}$ . This high diffusivity indicates that the icosahedral phase forms directly from the

liquid, consistent with the metastable phase diagram in Fig. 4.

## V. CONCLUSIONS

For the Al–Ru system we have developed a metastable phase diagram for rapid quenching from the liquid that includes the phase with icosahedral symmetry. The compositions of some of the phase boundaries were determined, but the temperatures were not measured and are shown schematically. The Al–Ru icosahedral phase is always found in the presence of other phases at the quench rates studied. It must form directly from the liquid state to account for the pronounced segregation of ruthenium to the icosahedral particles. Our metastable phase diagram is valid for the piston and anvil method of liquid quenching; it will be interesting to see how differences in cooling rates alter the features of the diagram.

## ACKNOWLEDGMENTS

We wish to acknowledge the expert microscopy work performed by both Chuck Echer of Lawrence Berkeley Laboratory and Carol Garland of the Caltech Materials Research Group. One of us (S.M.A.) wishes to acknowledge the Eastman Kodak and IBM corporations for financial support as well as discussions with W. L. Johnson, H. Fecht, and R. B. Schwarz and comments by the referees.

This work has been supported by the National

Science Foundation-Materials Research Groups Grant No. DMR 8421119. Work at Berkeley is supported by the United States Department of Energy under Contract No. DE-AC03-76SF00098.

## REFERENCES

- <sup>1</sup>D. Shechtman, I. A. Blech, D. Gratias, and J. W. Cahn, *Phys. Rev. Lett.* **53**, 1951 (1984).
- <sup>2</sup>See, for example, *J. Phys. (Paris)* **47**, Colloq. C3 (1986).
- <sup>3</sup>S. M. Anlage, P. Nash, R. Ramachandran, and R. B. Schwarz, *J. Less Common Met.* **136**, 237 (1988).
- <sup>4</sup>P. Pietrokowsky, *Rev. Sci. Instrum.* **34**, 445 (1963).
- <sup>5</sup>D. M. Kroeger, W. A. Coghlan, D. S. Easton, C. C. Koch, and J. O. Scarbrough, *J. Appl. Phys.* **53**, 1445 (1982).
- <sup>6</sup>J. H. Perepezko and W. J. Boettinger, in *Mater. Res. Soc. Symp. Proc.* **19**, 223 (1983).
- <sup>7</sup>Our measured value is somewhat less than the 3.2 at. % Ru determined from x-ray analysis of rapidly quenched dilute Al–Ru alloys by A. N. Varich and R. B. Lyukevich, *Izv. Acad. Sci. USSR, Met.* **1**, 73 (1973).
- <sup>8</sup>L. Edshammar, *Acta Chem. Scand.* **22**, 2374 (1968).
- <sup>9</sup>L. Edshammar, *Acta Chem. Scand.* **19**, 2124 (1965).
- <sup>10</sup>L. A. Bendersky and S. D. Ridder, *J. Mater. Res.* **1**, 405 (1986).
- <sup>11</sup>R. J. Schaefer, *Scr. Metall.* **20**, 1187 (1986).
- <sup>12</sup>J. A. Knapp and D. M. Follstaedt, *Phys. Rev. Lett.* **58**, 2454 (1987).
- <sup>13</sup>J. A. Knapp and D. M. Follstaedt (private communication).
- <sup>14</sup>The size distribution of icosahedral particles is rather sharp with a skew towards small particle sizes. For diffusion analysis, we chose to consider the largest particles because it is most likely that they formed early and were least affected by the diffusion fields of neighboring particles.